Membrane Topologies of Neuronal SNARE Folding Intermediates†

Chang Sup Kim, Dae-Hyuk Kweon, and Yeon-Kyun Shin*

Department of Biochemistry, Biophysics and Molecular Biology, Iowa State University, Ames, Iowa 50011

Received June 7, 2002; Revised Manuscript Received July 17, 2002

ABSTRACT: Assembly of the SNARE complex is essential for neurotransmitter release at synapses. Target plasma membrane SNAREs (t-SNAREs) syntaxin 1A and SNAP-25 form the t-SNARE complex that serves as an intermediate toward final SNARE assembly with vesicle-associated SNARE (v-SNARE). Membrane topologies of syntaxin 1A and the t-SNARE complex were investigated using site-directed spin labeling EPR. EPR analysis revealed that the basic region at the membrane−water interface is unstructured but inserted into the membrane. Such membrane insertion leaves no gap between the t-SNARE core and the membrane. Yet the lack of structure could provide the flexibility necessary for the t-SNARE core. Further, the insertion of the basic interfacial region into the membrane may have profound implications for the mechanism of SNARE-induced membrane fusion.

In eukaryotic cells, all vesicular transports, which deliver cargos to the designated destinations, utilize the same or similar conserved protein machinery that assists the fusion of vesicles to the target membrane. Soluble *N*-ethylmaleimide-sensitive factor attachment protein receptors (SNAREs)[1] are essential components of this fusion machinery (*1*−*4*). Assembly of vesicle-associated SNAREs (v-SNAREs) with the target membrane SNAREs (t-SNAREs) leads to membrane fusion.

In the neuron, syntaxin 1A and SNAP-25 are t-SNAREs residing on the synaptic plasma membrane. The t-SNARE proteins spontaneously assemble into a complex that is composed of two copies of transmembrane protein syntaxin 1A and one copy of peripheral membrane protein SNAP-25 (*5*), and the complex is believed to serve as the receptor for v-SNARE. Structurally, the "SNARE motifs", which are basically coiled coil sequences present in individual SNARE proteins, assemble into a four-stranded coiled coil (*6*, *7*).

Binding of v-SNARE to the t-SNARE complex leads to a similar but more stable four-stranded coiled coil structure (*8*, *9*) for which the SNARE motif from VAMP2 (vesicle-associated membrane protein 2) merely replaces one syntaxin component (*10*). The parallel coiled coil geometry has widely been considered to be important for membrane fusion (*9*, *11*, *12*). Theoretically, coiled coil formation could generate the inward force that induces the merge of two membranes (*13*−*15*), which eventually leads to membrane fusion. However, the manner in which the system harnesses the available energy has been the important question. The answer to this question could be found in the way the core complex is adjoined to the membrane.

In contrast to rapid advances in understanding the structure and function of SNARE soluble domains, progress has been very slow in determining the structure and topology of full-length SNARE proteins and their complexes. Recently, site-directed spin labeling EPR (*16*) makes it possible to investigate the membrane-bound full-length SNARE complex.

In this work, we report the structure and membrane topology of the syntaxin 1A dimer as well as those of the t-SNARE complex. These two t-SNARE states are considered to be folding intermediates toward the ternary SNARE complex (*17*). For EPR analysis, residues near the water−membrane interface were substituted with cysteine and modified with a nitroxide spin-label. The EPR distance measurement revealed that the interfacial linker region is disordered for both complexes. Further, the EPR accessibility measurement suggests that the basic interfacial region is inserted into the bilayer. The results provide insights into the way SNARE folding intermediates are adjoined to the membrane.

Functionally, homotypic membrane fusion has been observed in v-SNARE deleted systems (*18*−*20*), implying that the t-SNARE complex can mediate membrane fusion. It is also shown that t-SNARE proteins are sufficient for the fusion of ER membranes (*21*). Thus, the structure and topology of the t-SNARE complex presented in this work establish the structural basis for the possibility of t-SNARE-induced membrane fusion.

EXPERIMENTAL PROCEDURES

Protein Expression and Purification. Full-length syntaxin 1A (amino acids 4−288) and the C-terminal SNARE motif of SNAP-25 (SNAP-25[C]) (amino acids 125−206) were expressed in *Escherichia coli* as glutathione *S*-transferase (GST) fusion proteins and were purified using glutathione−agarose chromatography. The N-terminal SNARE motif of SNAP-25 (SNAP-25[N]) (amino acids 1−82) was expressed as a His_6-tagged protein and was purified using Ni−NTA resin (Qiagen).

Site-Directed Spin Labeling. For syntaxin 1A, three native cysteine residues (C145, C271, and C272) were changed to

† Support for this work is provided by National Institutes of Health Grant GM51290.

* To whom correspondence should be addressed. E-mail: colishin@iastate.edu. Phone: (515) 294-2530. Fax: (515) 294-0453.

[1] Abbreviations: EPR, electron paramagnetic resonance; GST, glutathione *S*-transferase; IPTG, isopropyl *β*-D-galactopyranoside; MTSSL, (1-oxyl-2,2,5,5-tetramethylpyroline-3-methyl)methanethiosulfonate spin-label; SNAP-25, synaptosome-associated protein of 25 kDa; SNARE, soluble *N*-ethylmaleimide-sensitive factor attachment protein receptor; VAMP2 (or v-SNARE), vesicle-associated membrane protein 2.

10.1021/bi026266v CCC: $22.00
Published on Web 08/10/2002

alanines to introduce a unique cysteine site specifically for the nitroxide attachment. Cysteine mutants were generated with the QuickChange site-directed mutagenesis kit (Stratagene), and they were confirmed by DNA sequencing. Cysteine mutants of syntaxin 1A were reacted with the (1-oxyl-2,2,5,5-tetramethylpyrrolinyl-3-methyl)methanethiosulfonate spin-label (MTSSL) while the protein is bound to the resin.

Preparation of the t-SNARE Complex. While His_6-tagged SNAP-25[N] was bound to Ni−agarose resin, an approximately 2-fold excess of other purified SNARE components (SNAP-25[C] and syntaxin 1A) was added to form the t-SNARE complex. The mixture was incubated at 4 °C for 24 h. After extensive washing had been carried out to remove the unbound proteins, the t-SNARE complex was eluted with a buffer containing 250 mM imidazole and 1% *n*-octyl glucoside (OG). The formation of the binary complex was confirmed with SDS−PAGE.

Membrane Reconstitution. Large unilamellar vesicles (LUV) 100 nm in diameter were prepared using an extruder as described elsewhere. Vesicles of 1-palmitoyl-2-oleoylphosphatidylcholine (POPC) containing 20 mol % 1-palmitoyl-2-oleoylphosphatidylglycerol (POPG) were first disturbed by *n*-octyl glucoside (1%) before addition of the detergent-dissolved SNAREs. After incubation for 2 h at room temperature, the detergent was removed by treating the solution with an excess of Bio-beads SM2 (Bio-Rad) at 4 °C overnight and for an additional 2 h with new beads. The final protein concentration was in the range of 30−50 μM.

EPR Data Collection. EPR spectra were obtained using a Bruker ESP 300 spectrometer equipped with a low-noise microwave amplifier (Miteq, Hauppauge, NY) and a loop-gap resonator (Medical Advances, Milwaukee, WI). The modulation amplitude was set at no greater than one-fourth of the line width. Spectra were collected at either room temperature or 130 K in the first-derivative mode.

EPR Distance Measurement. The low-temperature EPR spectra were analyzed using the Fourier deconvolution method to determine the interspin distance (*22*). When two nitroxides are separated by 25 Å, two spins interact with one another through the mechanism known as the spin−spin dipolar interaction. The dipolar interaction is dependent upon the distance by $1/r^3$, where r is the separation between the two nitroxides. For nitroxides in biological systems, the dipolar interaction effectively broadens the EPR lines. In the Fourier deconvolution analysis, the distance is determined by comparing the dipolar-broadened EPR spectrum with the noninteracting reference spectrum. We have used the Fourier deconvolution analysis routine that takes into account the distance distribution as a sum of two Gaussians (*23*).

EPR Accessibility Measurements. The gas exchange to the protein sample was achieved with the TPX EPR1 tube for the loop-gap resonator. For individual mutants, power saturation curves were obtained from the peak-to-peak amplitude of the central line ($M = 0$) of the first-derivative EPR spectrum as a function of incident microwave power in the range of 0.1−40 mW. Three power saturation curves were obtained after equilibration (1) with N_2, (2) with air (O_2), and (3) with N_2 in the presence of 200 mM NiEDDA (nickel ethylenediaminediacetic acid). From saturation curves, the microwave power $P_{1/2}$ where the first-derivative amplitude is reduced to one-half of its unsaturated value was calculated. The quantity $\Delta P_{1/2}$ is the difference in $P_{1/2}$ values in the presence and absence of a paramagnetic reagent. The $\Delta P_{1/2}$ value is proportional to the diffusion coefficient times the frequency of collision of the nitroxide with the freely diffusing reagents such as oxygen and NiEDDA. Thus, $\Delta P_{1/2}$ is considered to be equivalent to the accessibility W. The immersion depth is calculated on the basis of the reference curves determined from a set of lipid molecules spin-labeled at different acyl chain positions (*24*, *25*).

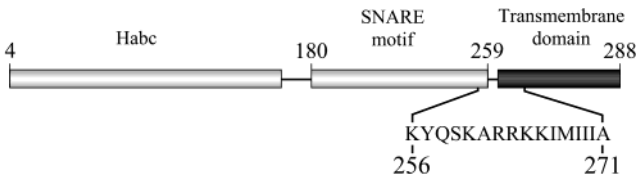

FIGURE 1: Structural elements of full-length syntaxin 1A. Habc is the α-helical domain that dissociates from the H3 domain upon SNARE complex assembly. The H3 domain of syntaxin 1A is the SNARE motif that participates in mediating the SNARE complex assembly. The site-directed spin labeling EPR experiment was carried out in the region of amino acids 256−271. The amino acid sequence of this region is displayed.

RESULTS

Site-Directed Spin Labeling and EPR Line Shape. To investigate the structure and membrane topology of syntaxin 1A as well as those of the t-SNARE complex, 16 consecutive residues of full-length syntaxin 1A near the membrane−water interface (amino acids 256−271) were replaced with cysteines using site-directed mutagenesis and cysteine mutants were modified with a nitroxide spin-label. The primary structure of syntaxin 1A and spin-labeled positions are shown in Figure 1. The characteristic feature of the interfacial region is the cluster of basic amino acid residues (RRKK). Spin-labeled proteins are reconstituted to POPC LUV containing 20 mol % POPG for EPR measurements.

EPR spectra of syntaxin 1A and those of the t-SNARE complex collected at room temperature are shown in Figure 2. EPR line shapes are relatively broad for all mutants, indicating slow motion. Slow motional spectra represent immobilized nitroxides (*26*, *27*). The immobilization could be due to the tertiary interactions with other parts of the protein or could result from the interaction with the lipid. Similar slow motional spectra are commonly observed for spin-labeled proteins when they are bound to the membrane (*28*−*30*).

EPR Distance Measurement. The EPR line shape is an excellent parameter for the tumbling rate of the nitroxide that often provides a qualitative assessment of the local environment surrounding the nitroxide (*26*, *27*). However, the line shape alone is, in most cases, not sufficient to yield the information pinpointing the secondary structure. For SNARE samples, we instead utilized the EPR distance measurement method (*22*, *23*, *31*) to identify the secondary structure of the interfacial region. It has been previously shown that full-length syntaxin 1A exists as dimers when bound to the membrane (*32*−*34*). Two copies of syntaxin 1A also exist in the t-SNARE complex (*6*, *7*). This is experimentally quite favorable, because single spin labeling on syntaxin 1A would result in two nitroxides in a protein molecule, and the distance between the pairs can be determined using the EPR distance measurement method.

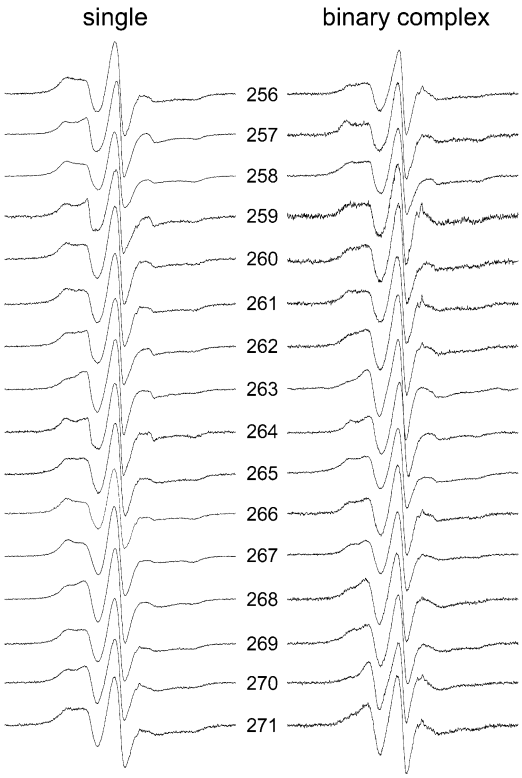

FIGURE 2: First-derivative EPR spectra. Room-temperature spectra of the spin-labeled syntaxin dimer are displayed on the left-hand side, and those of the t-SNARE complex are shown on the right-hand side.

To determine the interspin distance, EPR spectra were collected at low temperatures (~130 K). Although it is technically possible to measure distances at room temperature (*35*), we have chosen to analyze the low-temperature spectra in which motional broadening is effectively suppressed and the spectral broadening is exclusively due to spin−spin interactions (*22*). For all SNARE samples, we detect some spectral broadening in the low-temperature spectra (data not shown), indicating spin−spin interactions. EPR spectra taken for syntaxin 1A as well as those for the t-SNARE complex were analyzed using the Fourier deconvolution method to determine interspin distances. The Fourier deconvolution method has proven to be highly effective in determining the interspin distance in the range of 7−25 Å (*35*−*38*). The results are plotted in Figure 3.

We included in our EPR analysis several residues that are predicted to be part of the transmembrane domain (TMD), and we expect this region to be α-helical. On going from right to left in Figure 3, we encounter stronger spin−spin interactions and shorter distances for I269C, and again for K265C, for both systaxin 1A and the t-SNARE complex. Position 265 is four residues away from position 269, consistent with what is expected for α-helical geometry. These distance results support the interacting dimer model for TMDs of both systaxin 1A and the t-SNARE complex. Further, the data indicate that two TMDs are aligned in such a way that the helical face containing residues 265 and 269 are oriented toward one another.

On going further from right to left for the syntaxin dimer in Figure 3, we, however, observe nearly constant interspin distances (~17 Å) throughout the region of amino acids 256−264. This suggests that this region is most likely

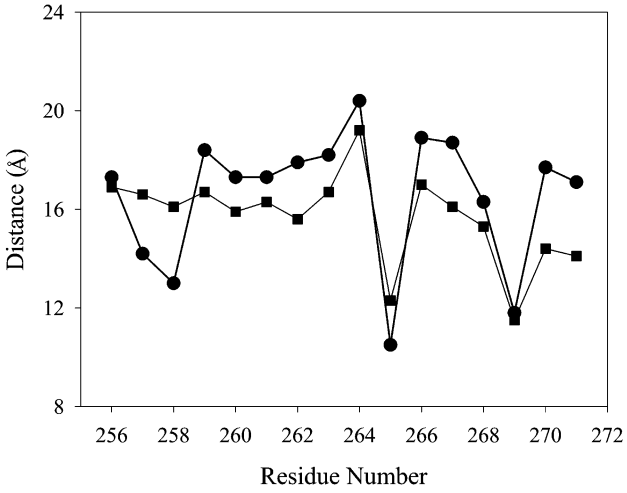

FIGURE 3: Interspin distance vs residue number for the syntaxin 1A dimer (■) and the t-SNARE complex (●).

nonhelical and unstructured. Similarly, for the t-SNARE complex, we do not observe any distance variation along the sequence in the range of residues 259−264 for the t-SNARE complex, indicating that this region might be unstructured, too. Importantly, however, we encounter again a shorter distance at position 258. Position 258 was shown to be an internal position in the structural model of the core domain (*9*). The shorter distance at position 258 suggests that this position belongs to the coiled coil and the core extends to residue 258 (or possibly to residue 259) in the full-length protein, similar to the prediction based on the structure of the soluble core.

EPR Accessibility Measurements. To investigate the membrane topology of the syntaxin 1A dimer as well as that of the t-SNARE complex, we have carried out EPR saturation experiments (*24*). This relaxation EPR technique has proven to be very effective in measuring the accessibility parameter and the membrane immersion depths (*39*−*41*). In panels A and B of Figure 4, the accessibility of nitroxide to a water-soluble paramagnetic reagent NiEDDA (W_{NiEDDA}) and that to the hydrophobic and membrane-favoring O_2 (W_{O_2}) are plotted versus residue number for the syntaxin dimer and the t-SNARE complex, respectively. In both panels, residues 256 and 257 exhibit high W_{NiEDDA} values, clearly indicating the solvent exposure of these positions. However, we observe a progressive decrease in the W_{NiEDDA} values along the sequence.

In contrast to the behavior of W_{NiEDDA}, we rather observe an overall progressive increase in the W_{O_2} values along the sequence, for both the syntaxin dimer and the t-SNARE complex. In particular, we observe a clear indication of the increasing W_{O_2} starting from position 260. The opposite trends of W_{NiEDDA} and W_{O_2} have been well documented and considered as a hallmark of the membrane-inserted polypeptide chain.

Using the test samples of known membrane immersion depths, it has been shown that the ratio of W_{NiEDDA} to W_{O_2} exhibits a quantitative relationship with respect to the membrane immersion depth (*24*). On the basis of the calibration curve from standard samples that include spin-labeled lipids and bacteriorhodopsin (*24*, *25*), we have determined the membrane immersion depths of spin-labeled SNARE samples. The results are plotted in Figure 5, and it

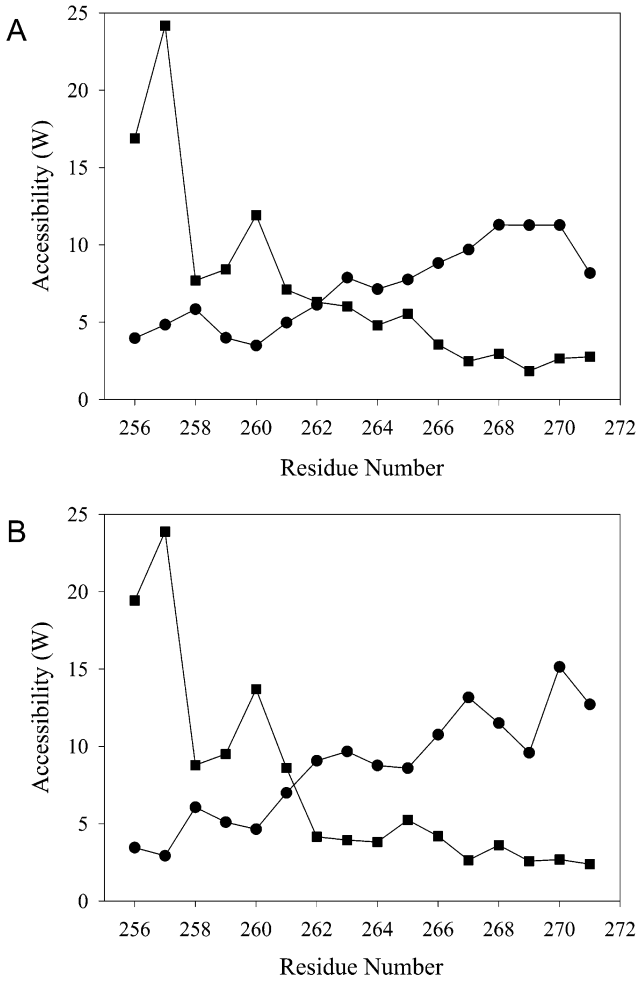

FIGURE 4: Accessibility to the paramagnetic reagents. (A) The accessibility to oxygen (W_{O_2}) (●) and that to NiEDDA (W_{NiEDDA}) (■) for syntaxin 1A are plotted vs residue number. (B) W_{O_2} (●) and W_{NiEDDA} for the t-SNARE (■) are plotted vs residue number.

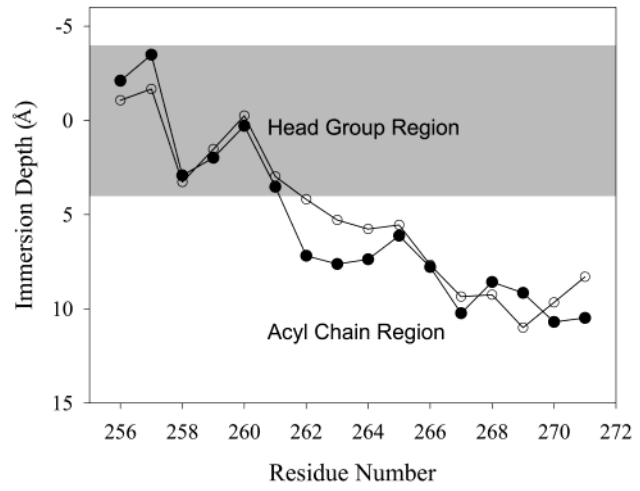

FIGURE 5: Membrane immersion depths for the nitroxides syntaxin 1A dimer (○) and the t-SNARE complex (●). In the graph, the location of the lipid phosphate groups is considered the 0 depth. The phosphate group is located right in the middle of the headgroup region which is approximately 8 Å thick. Only one leaflet of the bilayer is shown.

is clearly shown that the basic amino acid-rich interfacial region is buried in the membrane in both the syntaxin dimer and the t-SNARE complex.

Summary Results. Summarizing the EPR line shape analysis, interspin distances, and the accessibility data, we conclude that the interfacial region (amino acids 261−264 of syntaxin 1A) of SNARE folding intermediates is unstructured but inserted into the bilayer. Further, the distance data indicate that the TMD α-helix starts approximately from residue 265.

DISCUSSION

The membrane immersion depths shown in Figure 5 are approximate and must be interpreted with caution. This is largely because the accessibility values are strongly dependent upon the specific environment surrounding the given nitroxide. For this reason, the calibration based on the spin-labeled lipids and bacteriorhodopsin should be considered a semiquantitative scale for membrane immersion depths. Regardless, the high accessibility to oxygen and the low accessibility to NiEDDA observed for the interfacial positions (Figure 4) unambiguously demonstrate that nitroxides attached to this region are inserted into the membrane. Immobilized EPR line shapes (Figure 2) also support the membrane-inserted nitroxide side chain.

It is quite remarkable to find that the interfacial region (amino acids 260−265), which is highly hydrophilic with four positive residues (see Figure 1), is inserted into the membrane. Previously, it has been shown that the lateral mobility of the t-SNARE complex was retarded due to the acidic lipid−SNARE interactions (*42*). The insertion of the basic interfacial region into the membrane could facilitate such interactions. The insertion of basic peptides into the membrane has been discovered for many other systems, including the mitochondrial signal peptides (*43*), myristoylated alanine rich C-kinase substrate (MARCKS) peptides, and the synthetic model peptides (*44*).

High values of accessibility to oxygen for the nitroxides attached to the interfacial residues demonstrate that they are inserted into the acyl chain region of the bilayer, perhaps just underneath the headgroup region as indicated by the membrane immersion depths. One might argue that the hydrophobic nitroxide side chain could have an individual preference for the hydrophobic part of the membrane. Even in this case, we have to place the peptide backbone at least below the phosphate layer, taking into account the fact that the average arm length of the nitroxide side chain is on the order of 6−7 Å (*22*, *45*).

For the t-SNARE complex, the central coiled coil appears to be ordered up to residue 258, or possibly to residue 259. Further, we found that nearly all unstructured residues (amino acids 260−264) following the coiled coil are inserted into the membrane. Therefore, it seems that the core coiled coil is tightly attached to the membrane surface, yet the unstructured region may allow the movement for the coiled coil so that the t-SNARE core can orient in all directions on the membrane surface, which may play a role for the interaction with v-SNARE (Figure 6A).

For the syntaxin dimer, we found that the entire region preceding position 264 is unstructured, although it resumes being helical in TMD that perhaps starts from residue 265. In the crystal structure of the H3 domain, the coiled coil is ordered up to residue 254 (*46*), consistent with our finding with the full-length syntaxin. On the other hand, the EPR

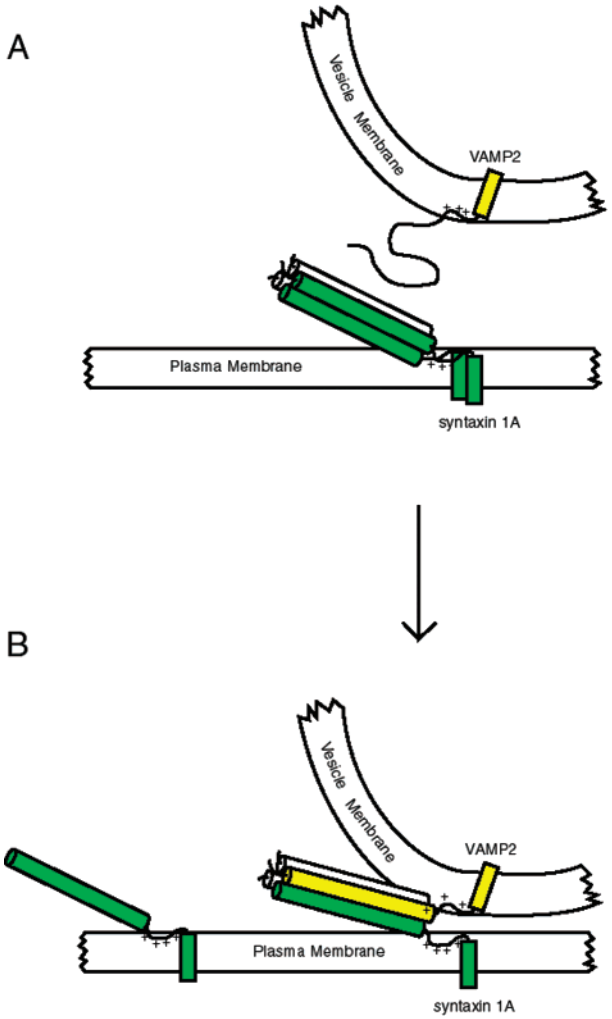

FIGURE 6: Proposed model for SNARE assembly. SNARE proteins are color-coded: syntaxin 1A (green), VAMP2 (yellow), and SNAP-25 (white). (A) The t-SNARE complex is a four-helix bundle on the plasma membrane. The membrane-inserted, yet unstructured, interfacial domain separating the core and TMD allows the positioning of the t-SNARE core to be favorable for the parallel alignment with v-SNARE. (B) Hypothetical model for the trans SNARE complex. The insertion of basic interfacial regions into the membrane provides tight coupling to two apposing membranes. Alternatively, the stress and strain at the junction may pull the interfacial domain out of the membrane, which may lift up the lipid molecules, facilitating fusion.

data suggest that residues following position 260 become immersed in the membrane. This means that four to five unstructured residues are above the level of the phosphate layer as a tether. Alternatively, it is possible that the syntaxin−syntaxin interaction is solely mediated by the TMD interactions, without the coiled coil formation of two H3 domains. Although this unstructured tether is expected to be flexible, EPR line shapes for those positions are relatively immobile. It is entirely possible that the short tether is still absorbed to the upper half of the headgroup region.

Possibly, in the SNARE folding pathway, SNAP-25 binds to the syntaxin dimer to form the t-SNARE complex. When the membrane topology of the syntaxin dimer and that of the t-SNARE complex are taken together, it appears that the binding of SNAP-25 to the syntaxin dimer stabilizes the C-terminal region of the core domain and makes the core domain directly coupled to the membrane surface. The EPR results suggest that the ARRKK region remains membrane-inserted during this process. According to the currently favored model, v-SNARE then replaces one copy of syntaxin in the t-SNARE complex to proceed to the SNARE complex (Figure 6). Another EPR study has shown that the ARRKK region remains to be inserted into the membrane in a recombinant ternary SNARE complex containing the SNARE motif of VAMP2 (*47*). Therefore, it is possible that the basic interfacial region is likely to stay membrane-inserted throughout the entire SNARE assembly process. However, previous studies with model basic peptides indicated that the energy of binding of the interfacial region of syntaxin 1A to the membrane is only a few kilocalories per mole (*48*). In reality, there must be high stress and strain in the trans SNARE complex. Thus, it is unclear whether the interfacial region can stay membrane-inserted or is pulled out of the membrane under the high strain during fusion.

It is quite intriguing that the v-SNARE-deleted system retains some fusion activity (*18*, *19*, *49*). One interpretation could be that the SNARE complex plays simply a catalytic role in controlling the speed of the fusion reaction. On the other hand, this raises the possibility of t-SNARE-induced membrane fusion. When previous studies (*6*) are combined with the results presented here, it appears that the t-SNARE complex is structurally fusion-competent. However, the t-SNARE complex is less stable than the ternary complex, making the t-SNARE complex a less effective fusogen.

Although the distance data are qualitatively consistent with the helical structure in TMD, the distance variation is much less than what is expected for a well-defined helix bundle (*50*). This could be due to some degree of disorder in the region. Alternatively, this could be due to the fluctuating structure near the unstructured interfacial region. In fact, we observe smeared intensities in EPR spectra (Figure 2), indicating the multiple conformational states or some conformational heterogeneity.

We note that the membrane immersion depths for positions in the transmembrane domain (residues 265−271) in Figure 5 appear to be somewhat inconsistent with those expected for a transmembrane domain with a perpendicular orientation. This might indicate that the membrane helix has a significant tilt.

CONCLUSIONS AND IMPLICATIONS

EPR results suggest that the basic polar interfacial region of t-SNARE complexes is unstructured but inserted into the membrane. Such insertion of the linker region into the membrane essentially leaves no gap between the t-SNARE core and the membrane, yet the lack of structure in this region could provide the necessary flexibility for the t-SNARE core. Such flexibility is necessary for the t-SNARE core to be able to assemble with v-SNARE into the all-parallel helix bundle (Figure 6A). Otherwise, the interaction with v-SNARE would be geometrically unfavorable.

Most importantly, the insertion of the linker region into the membrane may have profound implications for SNARE-induced membrane fusion. Membrane fusion requires the juxtaposition of two membranes. SNARE assembly to a parallel coiled coil will pull two membranes close to one another, similar to the case of viral fusion systems (*51*). However, the merging of two membranes requires as much as 25 kcal/mol of free energy (*52*). It is widely believed that

core complex formation generates the force that could be used for membrane deformation, but the manner in which the system harnesses the available force has been the fundamental question.

A hypothetical mechanism for membrane fusion has been proposed on the basis of the crystal structure of the SNARE core complex. In this model, α-helices of syntaxin 1A and VAMP2 in the core extend all the way through the transmembrane domains with a high degree of bending at the interfacial region (*9*).

On the basis of the EPR data, there is a possibility that the direct coupling between the core complex and the plasma membrane is achieved by the lateral insertion of the basic interfacial region into the membrane (Figure 6B). In support of this assertion, this segment was able to partially tolerate some helix-destabilizing mutations and amino acid insertions into the region (*13*, *53*). Alternatively, the high strain at the trans complex state may pull the basic interfacial domain out of the membrane, which may collaterally pull up some membrane divot. Importantly, the basic interfacial region is present in all transmembrane SNAREs, implying the generality of the functional role of the interfacial region.

ACKNOWLEDGMENT

We thank Fan Zhang for helping in the analysis of spin−spin distance measurement.

REFERENCES

1. Rothman, J. E. (1994) *Nature 372*, 55−63.
2. Jahn, R., and Südhof, T. C. (1999) *Annu. Rev. Biochem. 68*, 863−911.
3. Lin, R. C., and Scheller, R. H. (2000) *Annu. Rev. Cell Dev. Biol. 16*, 19−49.
4. Brunger, A. T. (2001) *Curr. Opin. Sturct. Biol. 11*, 163−173.
5. Fasshauer, D., Bruns, D., Shen, B., Jahn, R., and Brunger, A. T. (1997) *J. Biol. Chem. 272*, 4582−4590.
6. Xiao, W., Poirier, M. A., Bennett, M. K., and Shin, Y.-K. (2001) *Nat. Struct. Biol. 8*, 308−311.
7. Margittai, M., Fasshauer, D., Pabst, S., Jahn, R., and Langen, R. (2001) *J. Biol. Chem. 276*, 13169−13177.
8. Poirier, M. A., Xiao, W., Macosko, J. C., Chan, C., Shin, Y.-K., and Bennett, M. K. (1998) *Nat. Struct. Biol. 5*, 765−769.
9. Sutton, R. B., Fasshauer, D., Jahn, R., and Brunger, A. T. (1998) *Nature 395*, 347−353.
10. Fasshauer, D., Otto, H., Eliason, W. K., Jahn, R., and Brunger, A. T. (1997) *J. Biol. Chem. 272*, 28036−28041.
11. Lin, R. C., and Scheller, R. H. (1997) *Neuron 19*, 1087−1094.
12. Weber, T., Zemelman, B. V., McNew, J. A., Westermann, B., Gmachl, M., Parlati, F., Sollner, T. H., and Rothman, J. E. (1998) *Cell 92*, 759−772.
13. McNew, J. A., Weber, T., Engelman, D. M., Sollner, T. H., and Rothman, J. E. (1999) *Mol. Cell 4*, 415−421.
14. Wang, Y., Dulubova, I., Rizo, J., and Südhof, T. C. (2001) *J. Biol. Chem. 276*, 28598−28605.
15. McNew, J. A., Weber, T., Parlati, F., Johnston, R. J., Melia, T. J., Sollner, T. H., and Rothman, J. E. (2000) *J. Cell Biol. 150*, 105−117.
16. Hubbell, W. L., Gross, A., Langen, R., and Lietzow, M. A. (1998) *Curr. Opin. Struct. Biol. 8*, 649−656.
17. Fasshauer, D., Antonin, W., Subramaniam, V., and Jahn, R. (2002) *Nat. Struct. Biol. 9*, 144−151.
18. Nichols, B. J., Ungermann, C., Pelham, H. R., Wickner, W. T., and Haas, A. (1997) *Nature 387*, 199−202.
19. Marash, M., and Gerst, J. E. (2001) *EMBO J. 20*, 411−421.
20. Schoch, S., Deak, F., Konigstorfer, A., Mozhayeva, M., Sara, Y., Südhof, T. C., and Kavalali, E. T. (2001) *Science 294*, 1117−1122.
21. Patel, S. K., Indig, F. E., Olivieri, N., Levine, N. D., and Latterich, M. (1998) *Cell 92*, 611−620.
22. Rabenstein, M. D., and Shin, Y.-K. (1995) *Proc. Natl. Acad. Sci. U.S.A. 92*, 8239−8243.
23. Hall, J. A., Thorgeirsson, T. E., Liu, J., Shin, Y.-K., and Nikaido, H. (1997) *J. Biol. Chem. 272*, 17610−17614.
24. Altenbach, C., Greenhalgh, D. A., Khorana, H. G., and Hubbell, W. L. (1994) *Proc. Natl. Acad. Sci. U.S.A. 91*, 1667−1671.
25. Russell, C. J., Thorgeirsson, T. E., and Shin, Y.-K. (1999) *Biochemistry 38*, 337−346.
26. Mchaourab, H. S., Lietzow, M. A., Hideg, K., and Hubbell, W. L. (1996) *Biochemistry 35*, 7692−7704.
27. Schneider, D. J., and Freed, J. H. (1989) in *Biological Magnetic Resonance* (Berliner, L. J., and Reben, J., Eds.) Vol. 8, pp 1−76, Plenum, New York.
28. Kim, C.-H., Macosko, J. C., and Shin, Y.-K. (1998) *Biochemistry 37*, 137−144.
29. Perozo, E., Cortes, D. M., and Cuello, L. G. (1998) *Nat. Struct. Biol. 5*, 459−469.
30. Gross, A., and Hubbell, W. L. (2002) *Biochemistry 41*, 1123−1128.
31. Ottemann, K. M., Thorgeirsson, T. E., Kolodziej, A. F., Shin, Y.-K., and Koshland, D. E. (1998) *Biochemistry 37*, 7062−7069.
32. Margittai, M., Otto, H., and Jahn, R. (1999) *FEBS Lett. 446*, 40−44.
33. Laage, R., Rohde, J., Brosig, B., and Langosch, D. (2000) *J. Biol. Chem. 275*, 17481−17487.
34. Lerman, J. C., Robblee, J., Fairman, R., and Hughson, F. M. (2000) *Biochemistry 39*, 8470−8479.
35. Altenbach, C., Oh, K. J., Trabanino, R. J., Hideg, K., and Hubbell, W. L. (2001) *Biochemistry 40*, 15471−15482.
36. Thorgeirsson, T. E., Xiao, W., Brown, L. S., Needleman, R., Lanyi, J. K., and Shin, Y.-K. (1997) *J. Mol. Biol. 273*, 951−957.
37. Xiao, W., Brown, L. S., Needleman, R., Lanyi, J. K., and Shin, Y.-K. (2000) *J. Mol. Biol. 304*, 715−721.
38. Liu, Y.-S., Sompornpisut, P., and Perozo, E. (2001) *Nat. Struct. Biol. 8*, 883−887.
39. Shin, Y.-K., Levinthal, C., Levinthal, F., and Hubbell, W. L. (1993) *Science 259*, 960−963.
40. Altenbach, C., Marti, T., Khorana, H. G., and Hubbell, W. L. (1990) *Science 248*, 1088−1092.
41. Macosko, J. C., Kim, C.-H., and Shin, Y.-K. (1997) *J. Mol. Biol. 267*, 1139−1148.
42. Wagner, M. L., and Tamm, L. K. (2001) *Biophys. J. 81*, 266−275.
43. Yu, Y. G., Thorgeirsson, T. E., and Shin, Y.-K. (1994) *Biochemistry 33*, 14221−14226.
44. Victor, K. G., and Cafiso, D. S. (2001) *Biophys. J. 81*, 2241−2250.
45. Langen, R., Oh, K. J., Cascio, D., and Hubbell, W. L. (2000) *Biochemistry 39*, 8396−8405.
46. Misura, K. M., Scheller, R. H., and Weis, W. I. (2001) *J. Biol. Chem. 276*, 13273−13282.
47. Kweon, D.-H., Kim, C. S., and Shin, Y.-K. (2002) *Biochemistry 41*, 9264−9268.
48. Kim, J., Mosior, M., Chung, L. A., Wu, H., and McLaughlin, S. (1991) *Biophys. J. 60*, 135−148.
49. Schoch, S., Deak, F., Konigstorfer, A., Mozhayeva, M., Sara, Y., Sudhof, T. C., and Kavalali, E. T. (2001) *Science 294*, 1117−1122.
50. Zhang, F., Chen, Y., Kweon, D.-H., Kim, C. S., and Shin, Y.-K. (2002) *J. Biol. Chem. 277*, 24294−24298.
51. Eckert, D. M., and Kim, P. S. (2001) *Annu. Rev. Biochem. 70*, 777−810.
52. Kuzmin, P. I., Zimmerberg, J., Chizmadzhev, Y. A., and Cohen, F. S. (2001) *Proc. Natl. Acad. Sci. U.S.A. 98*, 7235−7240.
53. Wang, Y., Dulubova, I., Rizo, J., and Südhof, T. C. (2001) *J. Biol. Chem. 276*, 28598−28605.

BI026266V